

# The heavy quarkonium spectrum from quenched lattice QCD

Peter Boyle \*

*Department of Physics and Astronomy, University of Edinburgh, Edinburgh, UK*

**UKQCD Collaboration**

(August 9, 2018)

## Abstract

We present results of simulations of the quenched quarkonium spectrum at two values of the lattice spacing and for quark masses around  $m_c$  using the tadpole improved clover action. Attention is focussed on the lowest lying S and P states, and the triplet fine structure is obtained for the first time using a relativistic action.

Typeset using REVTeX

---

\*Present Address: Department of Physics and Astronomy, University of Glasgow, Glasgow

## I. INTRODUCTION

Lattice QCD simulations provide a systematically improvable method for predicting low energy phenomenology directly from QCD, providing a means to verify that QCD correctly reproduces experiment. We are primarily interested here in the simulation of charmonium, which remains a challenge for lattice QCD since the quark mass is sufficiently large to be difficult to resolve on coarse lattices, while the system is rather relativistic, causing problems for the NRQCD approach.

The angular momentum states calculated here are the  $^1S_0$ ,  $^3S_1$ ,  $^3P_0$ ,  $^3P_1$ , and  $^3P_2$  of lowest radial excitation. This is more extensive than typical lattice calculations using a relativistic action, which have generally been limited to the  $^1S_0$ ,  $^3S_1$  and spin-averaged S-P splittings [1–4], though Bhattacharya et al [5] produce a value for the  $\chi_{c1} - \chi_{c0}$  fine splitting using unimproved Wilson quarks.

### A. Simulation Techniques for Charm and Beauty

A discrete action approximating the continuum action is used, where finite differences are substituted for derivatives, summations for integrals and so on, giving the  $O(a)$  improved Wilson quark action [6,7]

$$S_{\text{latt}} = \frac{1}{2\kappa} \sum_{x,y} \bar{\psi}(x) M(x,y) \psi(y), \quad (1)$$

$$M(x,y) = \left[ 1 - \frac{i\kappa C_{SW} a g}{2} \sigma_{\mu\nu} F_{\mu\nu} \right] \delta_{x,y} - \kappa \sum_{\mu=1}^4 U_{\mu}(x) (1 - \gamma_{\mu}) \delta_{y,x+\mu} + U_{\mu}^{\dagger}(x - \mu) (1 + \gamma_{\mu}) \delta_{y,x-\mu}, \quad (2)$$

where  $\kappa = \frac{1}{2m_0 a + 8}$ , and the gauge group elements  $U_{\mu}(x) = e^{iagA_{\mu}(x + \frac{1}{2}\hat{\mu})}$ . An expansion of the discrete action in terms of continuum fields and their derivatives gives a natural classification of errors in powers of the lattice spacing  $a$

$$S_{\text{latt}} [\bar{\psi}(x), \psi(x), U_{\mu}(x)] = S_{\text{QCD}} [\bar{\psi}(x), \psi(x), A_{\mu}(x)] + aS_1 [\bar{\psi}(x), \psi(x), A_{\mu}(x)] + O(a^2). \quad (3)$$

We have chosen a lattice action which reduces to QCD as  $a \rightarrow 0$ , and may eliminate the leading errors due to  $S_1$  by adding appropriate (higher dimension) operators. The clover term

$$- \bar{\psi} C_{SW} \frac{ia g}{4} \sigma_{\mu\nu} F_{\mu\nu} \psi. \quad (4)$$

gives an  $O(a)$  contribution to the action so is irrelevant to the continuum limit; its coefficient may be selected to minimise the leading discretisation effects contained in  $S_1$ . The fixing of the clover coefficient has been performed in various ways - to different orders in perturbation theory [6–8], using mean-field improvement [9], and most recently using non-perturbative improvement criteria [10], giving a much improved continuum scaling behaviour of the light

hadron sector [11]. This categorisation of errors in powers of the lattice spacing  $a$ , however, introduces an upper limit for quark masses that can be accurately simulated,  $am_Q \ll O(1)$ . Within the quenched approximation contemporary simulations typically have  $am_{\text{charm}} \geq \frac{1}{2}$ , leaving them apparently susceptible to significant discretisation effects, which can only be removed by brute force extrapolation to the continuum limit. In recent years the problem of simulating heavy quarks in lattice QCD has therefore been tackled by discretising the effective theory, NRQCD – essentially performing a double (power counting) expansion in both the lattice spacing and in  $\frac{v^2}{c^2}$  [12], producing very wide ranging spectrum predictions for quarkonia [13–15]. However, the non-relativistic approach has recently been demonstrated to suffer from significant relativistic corrections for charmonium [16], leading to inconsistent results when comparing different orders of the nonrelativistic action [17], while the relativistic corrections to  $\Upsilon$  appear to be well under control.

If we make a power counting expansion, in the manner of Fermilab [1], of the improved Wilson action in both  $v^2$  and  $a$  simultaneously, however, we can see that the situation for heavy valence quarks is not as bad as naively supposed. Consider the tree-level low momentum expansion of the energy, (while this applies to the free case, the errors at large  $m_0 a$  are certainly indicative of errors in the interacting theory),

$$E(p) = m_1 + \frac{p^2}{2m_2} - \frac{i\sigma \cdot \mathbf{B}}{2m_B} + \frac{p^4}{8m_4^3} + A^{RS} + B^{SD} + \dots \quad (5)$$

where

$$am_1 = \log(1 + am_0), \quad (6)$$

$$am_2 = e^{am_1} \frac{\sinh(am_1)}{1 + \sinh(am_1)} \quad (7)$$

$$am_B = e^{am_1} \frac{\sinh(am_1)}{1 + C_{SW} \sinh(am_1)} \quad (8)$$

$$am_4 = e^{am_1} \frac{\sinh(am_1)}{\left[1 + e^{am_1} \sinh(am_1)(1 + \sinh^2(am_1)) + 2e^{2am_1} \sinh(am_1)\right]^{\frac{1}{3}}} \quad (9)$$

where the  $A^{RS}$  term violates rotational symmetry at  $O(\frac{1}{m^3})$  and  $B^{SD}$  contains order  $v^6$  spin-dependent corrections.

In this light, the accuracy of the action depends on both the size of  $am$  and on the size of  $v^2$ . In a sufficiently non-relativistic system the above Hamiltonian will, at tree level, accurately describe a particle of mass  $m_2 = m_B$ . If  $am \ll 1$  the action is approximately Lorentz symmetric <sup>1</sup> and the coefficients of higher order terms in the above non-relativistic

---

<sup>1</sup>assuming that  $a\Lambda_{QCD} \ll 1$

action will accurately match those of the continuum expansion. The essential point for charm however is that we have to estimate the size of errors in the subleading terms relative to the terms containing  $m_2$  and  $m_B$ . The errors will depend on both the difference between the higher order coefficient from that of the continuum Hamiltonian for a particle of mass  $m_2$ , and on the size of an  $O(v^{2n})$  prefactor. At tree level, therefore, we can estimate the fractional error introduced in the kinetic energy due to discretisation effects in the action as follows.

$$\Delta_{\text{kin}} = \frac{\frac{\langle p^4 \rangle}{8m_4^3} - \frac{\langle p^4 \rangle}{8m_2^3}}{\frac{\langle p^2 \rangle}{2m_2}} \quad (10)$$

Taking a charm quark mass of around 1.5 GeV and an estimate for  $\langle v^2 \rangle \simeq 0.3 \frac{am_{\text{charm}}}{am}$  (which approximates the data in [18] with sufficient accuracy to satisfy our needs), we plot the fractional error in the kinetic energy,  $\Delta_{\text{kin}}$  as a function of  $am$  for both of the lattice spacings we use in figure 1. The leading order error in the kinetic energy is estimated to be between 5% – 10%. We note that had we used the pole mass, the leading correction would have arisen from the  $m_1 - m_2$  discrepancy rather than the  $m_2 - m_4$  discrepancy, and therefore would not have been suppressed by  $v^2$ . Both analyses would, of course, have given the same continuum limit; however the use of  $m_2$  will for this reason have a milder lattice spacing dependence.

The disadvantage of any simulation involving Wilson quarks with  $am_0 \geq O(1)$  is that the  $a$  dependence of observables is not likely to have a simple low order polynomial form. There is no hierarchy in the orders of  $a$  due to terms  $(ma)^n$ ,<sup>2</sup> which is manifested in the non-linear dependence of the various mass definitions on the bare quark mass. These different mass definitions rapidly become identical as  $ma$  is reduced below 1, so that, for charm, studying the  $a$  dependence is sensible with current lattice spacings. For bottomonium results, however,  $am_0 \geq 1$  in both simulations, and we must rely on the power counting estimates of the correction terms to quantify errors. Continuum scaling plots provide only circumstantial evidence that the systematic errors in the bottom simulations are controlled. A more rigorous approach would be to form the union of bounds estimated for different error terms on each of the lattices; in this respect simulations in which  $am_0 \geq 1$  must be treated in a similar way to effective theories – the fact that the continuum limit exists for the Fermilab approach [1] is not in practice an advantage for bottom simulations since we do not know how to extrapolate *from this regime*.

Ideally we would make a corresponding estimate for the errors in the spin-dependent pieces of the action, but the subleading spin-dependent term for the Wilson action has not presently been calculated. However, it is thought that a similar size systematic error is likely in the spin-dependent Hamiltonian.

Some progress has recently been made in treating Wilson type quarks to one loop in perturbation theory for arbitrary quark mass. In particular Kronfeld et al [19] have calculated the 1-loop renormalisation of the terms  $m_1$  and  $m_2$ , showing that the discrepancy is

---

<sup>2</sup>we are dealing with on-shell correlation functions of valence quarks

dominated by the tree level result. The Kuramashi [20] calculation gave bilinear current renormalisation constants for Wilson quarks, and somewhat interestingly, noted that it was necessary to match  $m_2$  to the continuum pole mass in order to obtain the same IR behaviour for the vertex and wavefunction in the lattice theory as in the continuum theory. In order to obtain more rigorous control of the errors in charmonium simulations it would, of course, be interesting to have a one-loop calculation for  $m_4$ , and (at least) a tree level estimate of the subleading spin-dependent pieces for Wilson type actions.

In the remainder of this paper we present a study of quarkonium systems using the tadpole improved clover action [9,7] at both  $\beta = 6.0$  and  $\beta = 6.2$ , corresponding to  $a \simeq 0.1$  fm and  $a \simeq 0.07$  fm, analysed in the manner suggested by [1]. In the calculation at  $\beta = 6.0$  similar operators to those used in NRQCD calculations are applied enabling us to produce a wider ranging spectrum than previous relativistic calculations. The scaling behaviour of the hyperfine splitting between the two lattices is discussed, and estimates of the consistency of continuum quenched results with experiment are made. We note that while El-Khadra, Kronfeld, Mackenzie and others [1,19] propose improving the action for on shell quantities by breaking  $O(4)$  rotational symmetry in the Fermilab action, their simulations to date have involved the same re-interpretation of the standard relativistic quark action as we use here, and the results are therefore directly comparable.

## II. QUENCHED QUARKONIUM SPECTRUM AT $\beta = 6.0$

### A. Simulation Details - $\beta = 6.0$ calculation

The first simulation was performed using 499 sample gauge configurations from a quenched distribution at  $\beta = 6.0$  on a  $16^3 \times 48$  lattice. Five heavy quark masses were used, as given in Table I, with the tadpole improved clover action with  $C_{SW} = 1.47852$ , corresponding to  $u_0 = 0.8778$  taken from the plaquette.

The timesliced residue

$$|r_t|^2 = \frac{\sum_{x \in L^3} |\sum_{x', t'} M(x, t; x', t') \psi(x', t') - \eta(x, t)|^2}{\sum_{x \in L^3} |\psi(x, t)|^2}, \quad (11)$$

where the normalisation of the metric reflects the exponential fall off of the pseudoscalar correlator, was used to define the convergence criterion. Using the variance of previous simulation data to estimate the expected statistical error in the correlation functions, we found that requiring the timesliced residue on timeslice 24 ( the noisiest ) of  $r_{t=24} \leq O(10^{-11})$ , gives an error due to convergence when comparing to an extremely tightly converged propagator that is orders of magnitude below the expected variance. This was subsequently used as a convergence criterion and corresponds to a traditional residue of between  $10^{-8}$  and  $10^{-12}$  depending on the quark mass, significantly tighter than the  $10^{-7}$  obtainable using 32 bit precision.

Both local and fuzzed sources were used [21]. Fuzzed smearing uses Michael-Teper fuzzed links to covariantly transport the quark fields  $n$  links along each of the axes to form a face-centred cubic smearing function. The fuzzing radius  $n = 4$  was selected to optimise the

plateau for P-states using a small number of configurations, which, in combination with sink fuzzing, allowed a  $2 \times 2$  smearing matrix to be constructed,

$$\langle \mathcal{O}_i \mathcal{O}_j \rangle = \begin{pmatrix} \langle \mathcal{O}_L(x) \mathcal{O}_L(0) \rangle & \langle \mathcal{O}_F(x) \mathcal{O}_L(0) \rangle \\ \langle \mathcal{O}_L(x) \mathcal{O}_F(0) \rangle & \langle \mathcal{O}_F(x) \mathcal{O}_F(0) \rangle \end{pmatrix}. \quad (12)$$

Three additional propagators, from covariant derivative sources

$$\Delta_i(x) = \sum_y \left[ U_i(x) \delta(x + \hat{i}, y) - U_i^\dagger(x - \hat{i}) \delta(x - \hat{i}, y) \right] \delta(y, 0), \quad (13)$$

were generated at  $\kappa = 0.12600$ , lying closest to charm, allowing the differential operators in Table II to be constructed for mesons composed of this quark and one at another value of  $\kappa$ . The most important result of this is that we now have access to the angular momentum 2 P-state via the  $2^{++}$  operator, in both the  $T$  and  $E$  representations.

## B. Mass Fitting of Correlators

In what follows, all fits to correlators were made using correlated fits with the Marquardt Levenberg algorithm, and the bootstrap algorithm was used to estimate the errors, using 1000 bootstrap samples. Single exponential, row fit and matrix fit models were used.

The fit ranges were varied with  $t_{\max}$  holding typically three values selected by inspection of the effective mass plots, and  $t_{\min}$  varied over the entire range in which the Marquardt algorithm converged for the fit model. This procedure was carried out for each operator  $\mathcal{O} \in \{0^{-+}, 1^{--}, 0^{++}, 1^{++}, 1^{+-}\}$  and, where the data existed, for the  $2^{++}$  operator.

The information was used to select an optimal fitting range by considering the stability of the central value and error with varying  $t_{\min}$ , requiring  $Q \geq \mathcal{O}(0.1)$  and  $\chi^2/\text{dof} \leq \mathcal{O}(1.5)$ , and considering the consistency in the fitted masses between the double and single exponential fit methods.

The simultaneous double exponential fit to the fuzzed-source local-sink, and the local-local correlator was the selected method, and the ranges in Table III were deemed optimal. These were subsequently used to obtain the best fit masses in Table IV and Table V. The excited state masses given in these tables were not found to be sufficiently independent of the fit range to produce confident spectrum predictions. The effective mass plots obtained for the various angular momentum states of the  $\kappa_1 = \kappa_2 = 0.12600$  system are displayed in Figure 2 to Figure 4, where the open circles are the points from the local-local correlation function, and the fancy diamonds from the fuzzed-local. They are considered representative of the plots for other  $\kappa$  combinations.

Since the P-states have a large splitting from the pseudoscalar, the noise grows rapidly with time [22], and it is essential to perform part of the fit at early timeslices to obtain a good signal, requiring a well chosen fuzzing or smearing radius. Figure 4 clearly shows that we have resolved the complete fine structure of the  $\chi$  states for the first time with a relativistic action, since the 68% error bounds do not overlap. We, of course, obtain a reduced error by taking the bootstrapped difference in the fitted mass values.

### C. Kinetic Masses

The correlation functions were computed at various momenta allowing us to compute the kinetic mass by fitting the dispersion relation

$$E(p^2) = m_1 + \frac{p^2}{2m_2} + Cp^4. \quad (14)$$

The non-zero momentum behaviour of the (2600, 2600) pseudoscalar, Figure 5 is considered typical, and the fitted lattice kinetic masses are given in Table VII.

### D. Scale from Quarkonium S-P splitting

When quarkonia have been simulated (using either NRQCD or the heavy Wilson approach) quenched calculations have obtained a large slope in the  $\frac{1}{M}$  dependence of the spin-averaged  $1S - 1P$  splitting while the experimental splitting in  $\Upsilon$  and  $J/\psi$  is thought to differ by only a few MeV (with reasonable assumptions for the  $\eta_b$  mass). The slope calculated is a quenching effect [17]. It has been argued that the source of this slope is the incorrect running of the coupling in the quenched approximation [23,24] and that the definition of  $a^{-1}$  appropriate for quarkonia is that taken from the S-P splitting, in an attempt to eliminate quenching effects inherent in setting the scale from a low momentum quantity. This definition of the lattice spacing therefore depends on the mass of the heavy quarks used to determine it. The mass dependence of the quarkonium  $1P - 1S$  splitting and the corresponding inverse lattice spacing obtained in this simulation is shown in Figure 6. The inverse lattice spacings at  $\beta = 6.0$  obtained for  $J/\psi$  and  $\Upsilon$  are 2.17(6) GeV and 2.4(1) GeV respectively. The value obtained using NRQCD on the same lattice was 2.5(1) for the  $\Upsilon$  system [13]. The inverse lattice spacings obtained from  $M_\rho$  (with the tadpole improved action [25]) and  $\sqrt{K}$  are 1.96(4) GeV and 2.02(3) GeV respectively.

It has recently been suggested [18] based on potential models that the errors in the quenched quarkonium spectrum are dominated by an overestimation of the  $1S$  state relative to the physically larger states due to underestimation of the Coulomb coefficient in the quenched potential. As a result, even under a redefinition of the scale, the quenched quarkonium spectrum is inconsistent with experiment. For these reasons we analyse the  $\beta = 6.0$  simulation in three ways, using the  $\rho$  mass, the string tension, and the quarkonium S-P splitting to set the scale, the latter being included largely to allow comparison to other calculations. Finally we note that the sensitivity of both the hyperfine splitting and the  $S - P$  splitting to quenching makes them excellent candidates for observing unquenching effects in hadrons in exploratory dynamical simulations.

### E. Charm and Beauty Systems

The extrapolations in inverse heavy quark mass for the heavy-heavy systems were found to be amenable to a linear fit. The hyperfine splitting, S-P splitting and  $2^{++} - 1^{++} - 0^{++}$  fine structure were calculated and extrapolated to match the kinetic spin-averaged S-state

mass,  $M_2$ , to the physical mass, setting the scale using each of the string tension,  $M_\rho$ , or the S-P splitting. Here we artificially assume that the (experimentally unobserved)  $\eta_b$  mass lies 40 MeV below  $\Upsilon$  assuming linear fall in the hyperfine splitting from  $J/\psi$  with  $\frac{1}{M}$ . This will introduce at most an  $O(1/1000)$  error in the bare quark mass after fixing the mass of the spin-averaged S-state to the  $\Upsilon$  system.

### 1. Hyperfine Splitting

A linear potential model argument [26] gives the result that the quantity  $(M_v^2 - M_{ps}^2)$  is constant, and we compare the simulation data using  $M_2$  to define the  $(M_v + M_{ps})$  factor in Figure 7. Here we have included the light and heavy light data points obtained by UKQCD [27] on the same lattices, and we use  $M_1$  for the light data points.

Here  $M_\rho$  has been used to set the scale so that the data are normalised to experiment using  $M_\rho^2 - M_\pi^2$ , and the overall shape is significant. The experimental points are approximately constant for the light and heavy-light systems, while lying slightly higher for  $J/\psi$ . This probably results from the quarkonium S-states being significantly determined by the Coulomb part of the potential. The simulation data are very flat above the  $D$  meson and the quarkonium points do not demonstrate the “emergent” behaviour shown by experiment, which we attribute to the Coulomb pole increasing the wavefunction at the origin. Since the data is normalised to experiment at the light quark end of the plot, it appears that in the quenched approximation the hyperfine splittings fall disproportionately quickly with quark mass when compared with the real world in the  $\pi$ ,  $K$ ,  $D$  sector.

Figure 8 presents the extrapolation of the quarkonium hyperfine splitting to charm and beauty using the string tension to scale both axes in the extrapolation. The mass dependence of the splitting is a straight line through the origin, in agreement with the non-relativistic expansion of QCD, and in contrast to the extrapolations obtained with the tree-level clover and unimproved Wilson actions, [28,2], as seen in Figure 9. The size of the hyperfine splitting is in clear disagreement with that in the  $J/\psi$  system.

### 2. Fine Structure

We compute the P-states using the  $\gamma$ -based operators where possible; they were found to be significantly statistically cleaner, as can be seen by comparing figures 3 and 4. Furthermore data existed for the degenerate quarkonium with the  $\gamma$  operators for each of the  $\kappa$  values. The  $2^{++}$  state, however, required extra derivative source propagators for one of the quarks in the meson; these were generated only for  $\kappa = 0.12600$ , so that the fine splittings involving the  $2^{++}$  state were extrapolated linearly using non-degenerate mesons, to the point where the non-degenerate pseudoscalar inverse kinetic mass was equal to the  $\eta_c$  mass. We generated correlation functions for operators in both the  $T_2$  and  $E$  representations and found them to be degenerate within our statistical error. We take the fitted mass from the  $T_2$  representation which we found to be statistically slightly cleaner.

This analysis is not ideal but errors introduced may be estimated using the non-degenerate Hamiltonian in [29]. This is easily re-written in terms of the combinations  $(m_1 + m_2)$  and  $(m_1 - m_2)$  giving that the corrections to the fine structure Hamiltonian



for non-degenerate quarks are proportional to  $\frac{m_1 - m_2}{m_1 + m_2}$ . In extrapolating to charm from the nearby  $\kappa = 0.12600$ , the correction to the fine splitting is of order 10%, which is lower than the level of statistical error. Extrapolations to the beauty systems via this method however are problematic.

The extrapolations are performed using degenerate quarks and the  $\gamma$ -based operators for splittings not involving the  $2^{++}$  state. The  $m_Q$  dependence of the fine structure is shown in Figures 10, 11, 12 and 13. As can be seen, we resolve completely the  $\chi$  triplet, however, the calculated splitting between the  $h_c$  and  $\chi_{c1}$  is consistent with zero. We obtain estimates for the ratio  $\frac{M(^3P_2) - M(^3P_1)}{M(^3P_1) - M(^3P_0)}$  of 1.6(6) for charmonium and the systematics in extrapolating to bottomonium leave the extrapolation not worth considering here. The experimental value is 0.48 for charmonium and 0.66 for bottomonium. The same splitting when calculated in NRQCD has been shown to suffer from significant discretisation effects [17], so that without calculation of the same quantity at other lattice spacings we cannot distinguish between discretisation and quenching effects.

### 3. Spectrum Predictions

The results obtained using each of the string tension, the  $\rho$  mass, and the quarkonium S-P splitting, extrapolated to both the  $J/\psi$  and  $\Upsilon$  systems can be found in Table VIII. As an illustration of the resulting data we present diagrams for the spectrum obtained using the string tension for both the  $J/\psi$ , Figure 14, and the  $\Upsilon$ , Figure 15, systems. The spectrum obtained for  $J/\psi$  is broadly comparable to experiment, with the spin splittings underestimated, while we expect  $\Upsilon$  the results show severe quenching effects in both the hyperfine and  $S - P$  splittings.

Our values for the hyperfine splitting in charmonium however, agree with the FNAL quenched data which has been included in reviews by Shigemitsu [30] and Davies [17]. For both systems the discrepancies in the fine structure may well include strong discretisation effects. It is common for the lattice spacing to be set independently in each of the  $J/\psi$  and  $\Upsilon$  systems via the  $S - P$  splitting at that quark mass. This would certainly improve the spectrum diagram we obtain for  $\Upsilon$ , however it is felt that, since this defines a different quenched theory for each system, this obscures the fact that the one quenched theory cannot simultaneously reproduce the spectra of these systems. Previous calculations of charmonium P-states with a relativistic lattice action have been made [5,31,27,32], however, this is the first relativistic lattice calculation that completely resolves the  $\chi$  triplet.

## III. SCALING BEHAVIOUR OF HYPERFINE SPLITTING

We also performed a less extensive calculation using the tadpole-improved clover action at  $\beta = 6.2$ , where we consider only the S-states. The simulation used 150 sample gauge configurations from a quenched distribution at  $\beta = 6.2$  on a  $24^3 \times 48$  lattice. Five heavy quark masses corresponding to,

$$\kappa_{\text{heavy}} \in \{0.12000, 0.12300, 0.12600, 0.12900, 0.13200\},$$

were used, all having the tadpole improved clover action with  $C_{SW} = 1.44239$ , corresponding to  $u_0 = 0.88506$  taken from the plaquette. The data were fitted using a similar procedure to that described previously.

With only two calculations, an extrapolation to the continuum using a linear model is ill-advised, and so we plot the lattice spacing dependence without performing a fit. The scaling behaviour of the  $J/\psi$  hyperfine splitting is shown in Figure 16, and can be seen to be near scaling with both the string tension and  $M_\rho$  scales, in clear disagreement with experiment. The charmonium hyperfine results are consistent with those of El-Khadra et al [1]. Based on this it is reasonable to assume that our results on the  $\Upsilon$  hyperfine splitting underestimate the (as yet undetermined) experimental value.

Future calculations should produce a result for the hyperfine splitting which scales using the quarkonium S-P splitting to set the lattice spacing. This will probably not agree with those using the low momentum observables since NRQCD calculations produce a result [17] for the S-P splitting in units of  $M_\rho$  which scales and is 30% lower than experiment for  $\Upsilon$ ; this induces an inconsistency between the quarkonium hyperfine splitting scaled with each of these quantities. The mass dependence of the quenched S-P splitting will, of course, mean that the level of discrepancy between the lattice spacing definitions will differ in the  $J/\psi$  and  $\Upsilon$  systems. For comparison we can estimate the value NRQCD calculations of the hyperfine splitting would yield using  $M_\rho$  to set the scale by assuming  $\Delta_{\text{hyperfine}} \propto \frac{1}{m_Q}$ ; feeding the change in scale into both the selected quark mass and the splitting then yields a 40-50% reduction in the hyperfine splitting. The NRQCD quenched continuum result appears to be around 35 MeV [17] using the S-P splitting to set the scale, with a 30% uncertainty due to  $u_0$  ambiguities and higher order relativistic corrections. This gives an estimate for the central value of around 17-21 MeV if  $M_\rho$  were used to set the scale.

#### IV. CHARM QUARK MASS

We first fix the bare lattice mass,  $\kappa_{charm}$ , by requiring the kinetic mass of the pseudoscalar matches that of the  $\eta_c$  using the string tension to set the scale. We then obtain values for the pole mass of the charm quark using two methods [33] involving either  $m_1$  or  $m_2$ , which differ due to lattice spacing effects.

The first method evaluates the binding energy at that bare quark mass:

$$aB_1 = aM_1(Q\bar{Q}) - 2aM_{1Q}^{PT}, \quad (15)$$

where the perturbative pole mass contains its one loop correction obtained from [19]

$$aM_{1Q}^{PT} = \sum_{l=0}^1 g^{2l} aM_1^{[l]} \quad (16)$$

The binding energy, defined via  $M_1$ , is then subtracted from the physical meson mass to give the charm pole mass.

$$M_{\text{ch}}^{\text{pole}} = M(1S) - B_1 \quad (17)$$

The other method employed relates the one loop kinetic mass to the bare quark mass using the all orders in  $am_Q$  renormalisation constant [19].

$$M_2 = Z_{M_2} \times m_2(M_1^{PT}), \quad (18)$$

where  $M_1^{PT}$  contains its one loop correction and

$$m_2(aM_1) = e^{aM_1} \frac{\sinh aM_1}{1 + \sinh aM_1} \quad (19)$$

The largest source of error in the calculation is the coupling  $g^2$ . Ideally we use the Brodsky-Lepage-Mackenzie scale  $q^*$  for the self-energy. We have not however evaluated this scale and instead proceed in a similar manner to [34,35] by varying the scale at which we evaluate  $\alpha_V(q)$  over the range  $\frac{1}{2a} \leq q \leq \frac{2}{a}$  to estimate the likely higher order error.

The scaling behaviour obtained for the two methods for obtaining the charm pole mass is given in Figure 17. The error is dominated by the uncertainty in the coupling, however it is plausible that a consistent continuum limit is reached by the two methods, and suggest the likely range for the pole mass is  $1.25 \text{ GeV} \leq m_{ch}^{\text{pole}} \leq 1.55 \text{ GeV}$ . We find the pole mass is, naturally, rather insensitive to the upper limit of  $q$  and strongly sensitive to the lower limit on  $q$  due to the nature of the running coupling.

We note that the perturbative errors are large here, in particular Gray et al [37] find a large  $O(\alpha_s^2)$  correction in the relation between the pole and  $\overline{MS}$  masses. Due to this uncertainty we do not convert our results to  $\overline{MS}$  and instead quote only the pole mass. This is not to say, of course, that we believe that the pole mass is better defined, but rather we are reluctant to apply the one loop formula when a large two loop correction may exist.

## V. CONCLUSIONS

The quenched hyperfine splittings in quarkonium systems scale within statistical error between the two calculations with either the string tension or  $M_\rho$  used to set the scale, and are in clear disagreement with experiment for  $J/\psi$  and with phenomenological model predictions for  $\Upsilon$ . Our results for the hyperfine splitting in charmonium are in agreement with [1], and those for  $\Upsilon$  are in plausible agreement with NRQCD results when a correction for the different inverse lattice spacings used is made. Systematic errors are estimated to be at the 5% level.

We make the first lattice calculation of the complete  $1P$  triplet fine structure using a relativistic quark action, and find that the inconsistencies of the spectrum with experiment in the calculation at  $\beta = 6.0$ , namely the low hyperfine splitting and the mass dependence of the  $S - P$  splitting are consistently explicable by an underestimation of the Coulomb coefficient at hadronic length scales in the quenched approximation. We give an estimate for the pole mass of the charm quark, with an error which is dominated by perturbative uncertainties.

## VI. ACKNOWLEDGEMENTS

We acknowledge the support of EPSRC grant GR/K41663 and PPARC grant GR/K55745. The calculations were performed using UKQCD time on the Cray T3D in the EPCC at the University of Edinburgh. Peter Boyle was funded by the Carnegie Trust for the Universities of Scotland while this work was carried out at the University of Edinburgh, and is grateful for PPARC grant PP/CBA/62 and both the University of Glasgow, and University of California, Santa Barbara, where this work was written up. I acknowledge many useful conversations with Christine Davies during the course of this work.

## REFERENCES

- [1] A. El-Khadra et al, Physical Review D55 3933 (1997).
- [2] C. Allton et al, Phys. Lett. B292 408 (1992).
- [3] S. Collins et al, Nucl. Phys B47 (Proc Suppl) 455 (1996).
- [4] M. Wingate et al, Physical Review D52 307 (1995).
- [5] T. Bhattacharya et al, Physical Review D53 6486 (1996).
- [6] B. Sheikholeslami and R. Wohlert, Nuclear Physics B259 572 1985
- [7] G. Heatlie et al, Nuclear Physics B352 266 (1991).
- [8] R. Wohlert, DESY preprint 87-069 (1987) Unpublished  
S. Naik, Phys.Lett. B311 (1993) 230-234  
M. Luscher, P. Weisz, Nuclear Physics B479 (1996) 429-458
- [9] P. Lepage and P. Mackenzie, Physical Review D48 2250 (1993).
- [10] M. Luscher et al, Nuclear Physics B491 (1997) 323-343
- [11] Hartmut Wittig, Nuclear Physics B63 (ProcSuppl) 47, 1998.
- [12] W.E. Caswell, G.P. Lepage, Phys.Lett. B167, 437, 1986
- [13] C. Davies et al, Physical Review D50 6963 (1994).
- [14] C. Davies et al, Physics Review D52 6519 (1995).
- [15] C. Davies et al, Physics Letters B382 131 (1996).
- [16] H. Trotter, Physical Review D55 6844 (1997).
- [17] C. Davies, Nuclear Physics (Proc Suppl) A60, 124, 1998 .
- [18] G. Bali, P. Boyle, hep-lat/9809180. To be published in Physical Review D.
- [19] B.P. Mertens, A. Kronfeld, A. El-Khadra. Physical Review D58, 34505, 1998.
- [20] Y. Kuramashi, Phys. Rev. D 58 (1998) 34507.
- [21] P. Lacock et al, Physical Review D51, 6403, 1995.
- [22] P. Van Baal and A. Kronfeld, Nuclear Physics (Proc Suppl) B9 (1989) 227.
- [23] A. El-Khadra, G. Hockney, A. Kronfeld, P. Mackenzie. Dallas HEP 1992:1523-1528.
- [24] S. Aoki et al. Nuclear Physics (Proc Suppl) 60A (1998) 114.
- [25] P. Rowland. PhD Thesis, and UKQCD Collaboration *in preparation*.
- [26] W. Lucha, Phys. Rep. 200:127 (1991).
- [27] P. Boyle, UKQCD Collaboration, Nuclear Physics (Proc Suppl) B63 (1998) 314.
- [28] S. Collins, PhD Thesis, The University of Edinburgh (1993).
- [29] W. Lucha, Lecture Course, Development in Nuclear Theory and Particle Physics Summer School, Dubna, 1995. hep-ph/9601263.
- [30] J. Shigemitsu, Nucl. Phys. B53 (Proc Suppl) 16 (1997).
- [31] P. Boyle, UKQCD Collaboration, Nuclear Physics (Proc Suppl) B53 (1997) 398.
- [32] P. Mackenzie et al, Nuclear Physics (Proc Suppl) B63 (1998) 398.
- [33] A. Kronfeld, Nuclear Physics (Proc Suppl) 63 (1998) 311.
- [34] R. Gupta, T. Bhattacharya, Physical Review D55 (1997) 7203.
- [35] C. Allton et al, Nuclear Physics B431 (1994) 667.
- [36] V. Gimenez et al, Nuclear Physics B540, (1999) 472.
- [37] N. Gray et al, Z. Phys. C48 673 (1990).

## FIGURES

FIG. 1. Estimated error in mean kinetic energy estimated at tree level as a fraction of the total kinetic energy,  $\Delta_{\text{kin}}$  at  $\beta = 6.0$  and  $\beta = 6.2$  due to discretisation effects. We used an approximation to potential model values  $\langle v^2 \rangle$  in this estimate. Estimated systematic errors are of the order 5%.

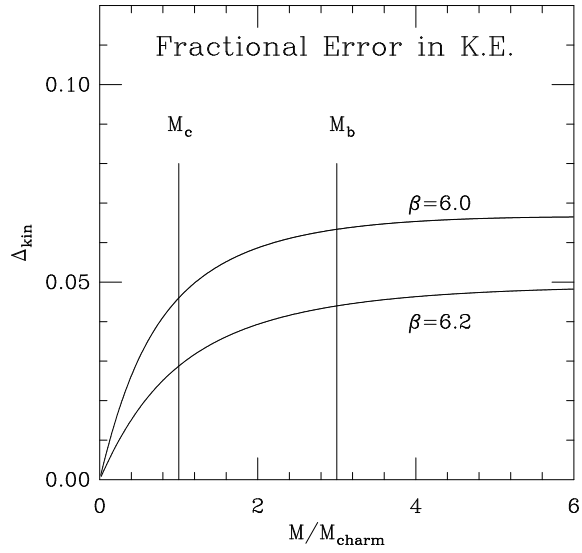


FIG. 2. Heavy-heavy pseudoscalar and vector effective masses for a meson containing degenerate quarks with  $\kappa = 0.12600$  at  $\beta = 6.0$ . These plots are considered representative of the rest of the data set. The hyperfine splitting is clearly seen. The circles are points from local-local correlation functions, and the fancy squares come from the fuzzed source, local sink correlation functions.

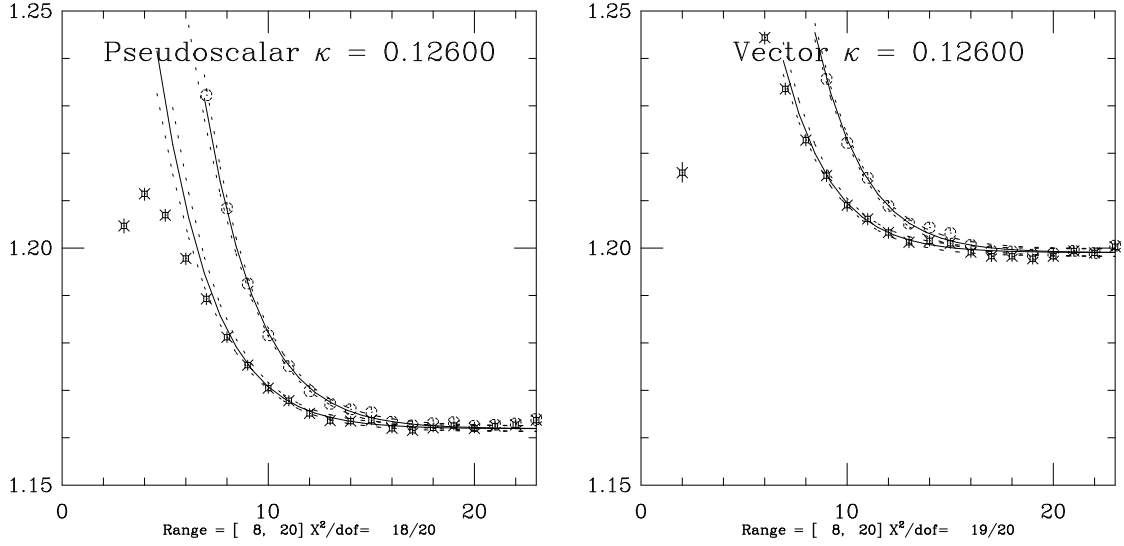


FIG. 3. Quarkonium  $\chi_0, \chi_1$ , and  $h$  states using  $\gamma$  operators for a meson containing degenerate quarks with  $\kappa = 0.12600$  at  $\beta = 6.0$ . The  $0^+ - 1^+$  splitting can be clearly seen. The  $1^{++}$  and  $1^{+-}$  states are not resolved. The circles are points from local-local correlation functions, and the fancy squares come from the fuzzed source, local sink correlation functions.

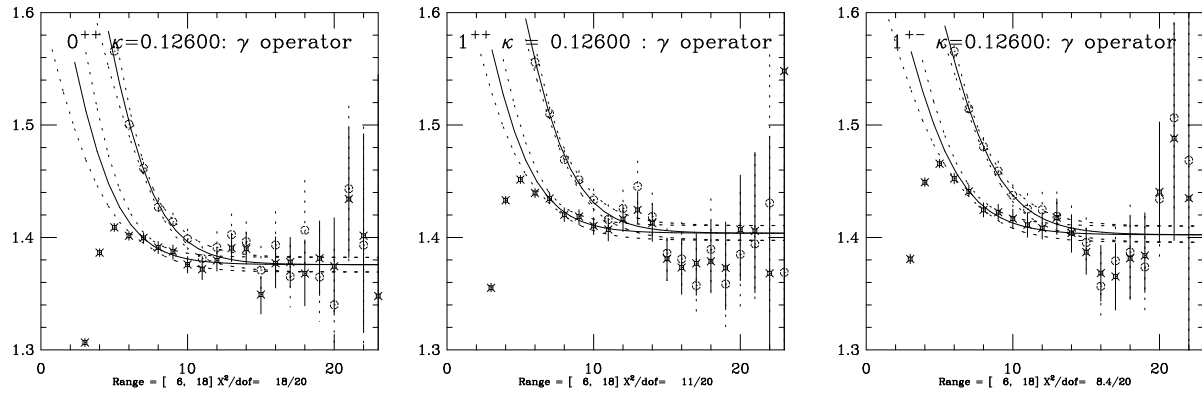


FIG. 4. Quarkonium  $\chi_0, \chi_1$ , and  $\chi_2$  states using differential operators for meson containing degenerate quarks with  $\kappa = 0.12600$  at  $\beta = 6.0$ . The complete fine structure of the  $\chi$  triplet is clearly resolved, even before correlated differences are taken.

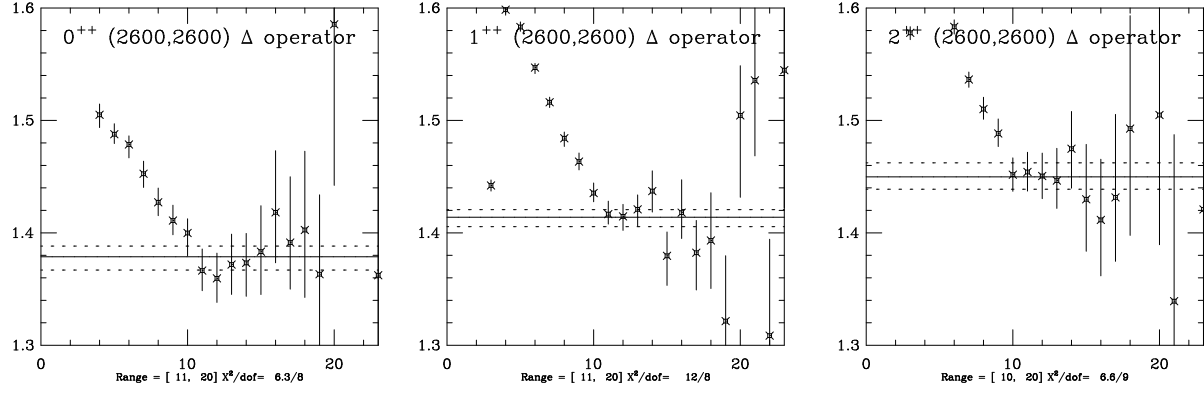


FIG. 5. Fit to the dispersion relation for the pseudoscalar meson containing degenerate quarks with  $\kappa = 0.12600$  at  $\beta = 6.0$ . The fit is quadratic, and a significant difference between the fitted  $p^2$  coefficient and the naive derivative obtained from the first two points is found, making the quadratic fit necessary.

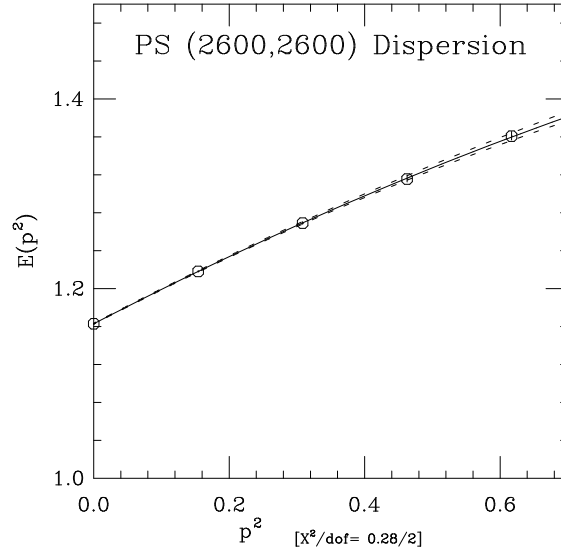




FIG. 6. Plots show the  $S - P$  scaled to the string tension at  $\beta = 6.0$ , and the inverse lattice spacing obtained from quarkonium  $S - P$  splitting as a function of the inverse kinetic pseudoscalar meson mass. No significant deviations from linearity are found within statistical error.

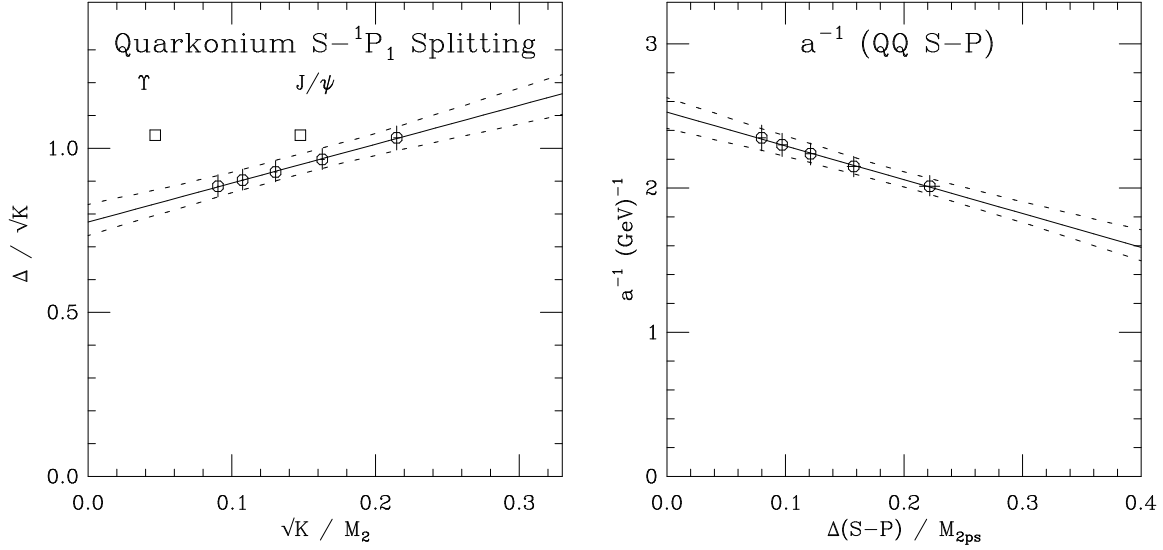


FIG. 7. Hyperfine splitting across entire mass range at  $\beta = 6.0$ . The first three data points are degenerate light quarks (open circles), there are fifteen heavy-light data points (fancy diamonds), and five degenerate heavy-heavy data points (fancy squares). The heavy-heavy points show no sign of a rise relative to heavy-light points, in contrast to the experimental behaviour. This shows a clear defect of the quenched approximation. Here we have factorised  $m_V^2 - m_{PS}^2$  and used a kinetic mass factor  $m_2(PS) + m_2(V)$  and a pole mass factor  $m_1(V) - m_1(PS)$  for all but the light quarks, for which we use solely  $m_1$  terms.

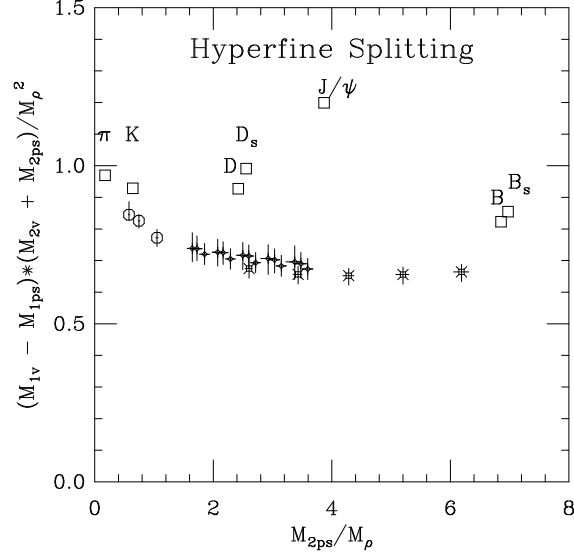


FIG. 8. Extrapolation of quarkonium hyperfine splitting in the inverse pseudoscalar meson mass at  $\beta = 6.0$ . The axes in this plot are scaled to the string tension. The ratio of the hyperfine splitting to the string tension is clearly underestimated by the data compared with experiment. The hyperfine splitting extrapolates to zero in the static limit. The axes are scaled using the string tension.

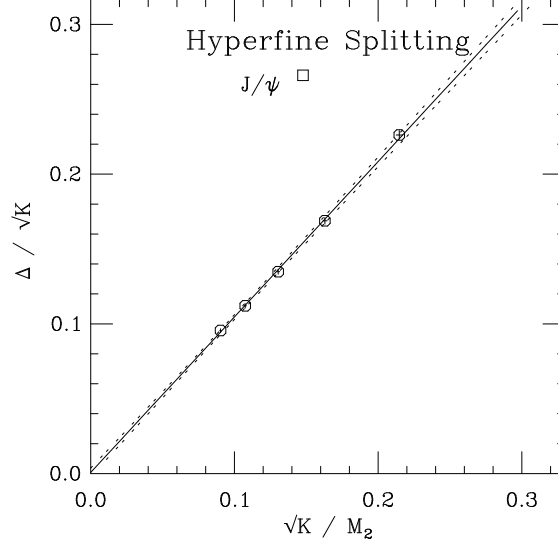


FIG. 9. Previous UKQCD heavy quark extrapolation of quarkonium hyperfine splitting using various actions. The hyperfine splitting clearly disappears before the static limit, in contrast to the tadpole improved data set.

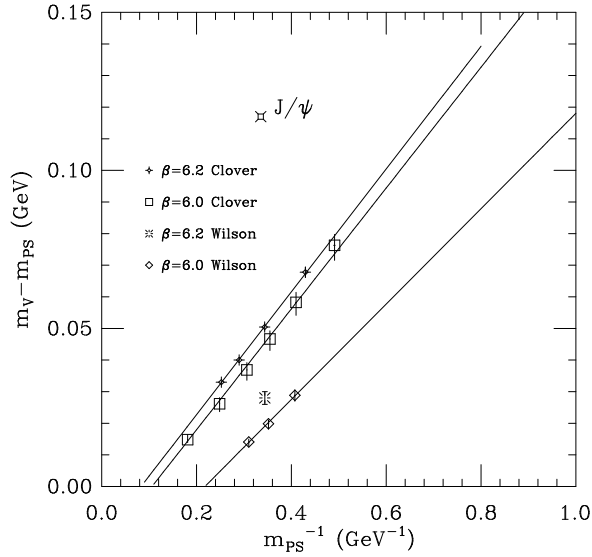


FIG. 10. Heavy quark extrapolation of the quarkonium  $\chi_{c1} - \chi_{c0}$  fine splitting at  $\beta = 6.0$  using degenerate quarks and the  $\gamma$  operators. This splitting is clearly non-zero, but appears to be significantly underestimated at this lattice spacing. Whether this effect is due to quenching or discretisation errors cannot be understood without corresponding simulations on other lattice spacings. The axes are scaled using the string tension.

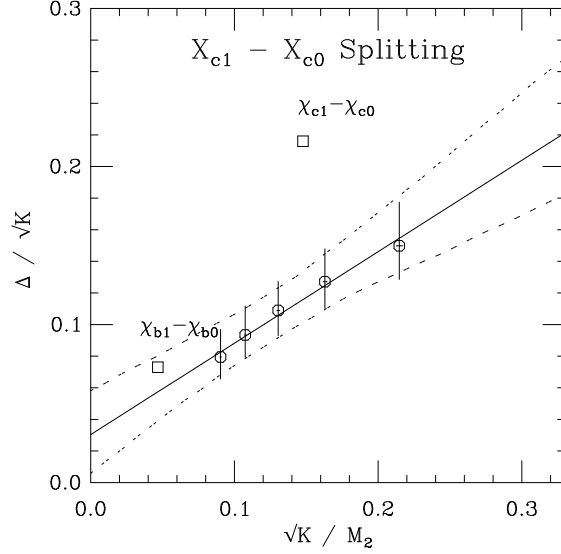


FIG. 11. Heavy quark extrapolation of quarkonium  $\chi_{c1} - h_c$  fine splitting at  $\beta = 6.0$  using degenerate quarks and the  $\gamma$  operators. This is statistically consistent with zero at all masses simulated. The axes are scaled using the string tension.

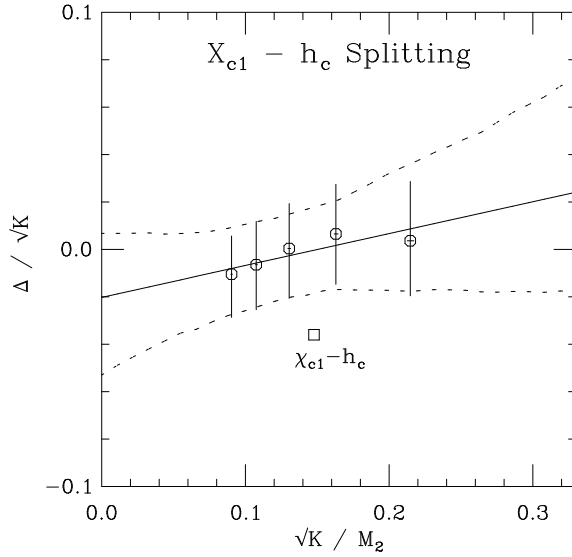


FIG. 12. Heavy quark extrapolation of quarkonium  $\chi_{c2} - h_c$  fine splitting at  $\beta = 6.0$ . Here we use non-degenerate quarks  $\kappa_1 \in \{0.114, 0.118, 0.122, 0.126\}$  and  $\kappa_2 = 0.126$ , and plot the difference between the mass of the  $2^{++}$  state using the differential operator and the  $1^{++}$  using the  $\gamma$  operator versus the inverse kinetic mass of the corresponding pseudoscalar meson. The systematic errors in making predictions for degenerate quarkonia are expected to be below statistical errors for  $c\bar{c}$ , but are poorly controlled for  $b\bar{b}$ . The results are scaled using the string tension.

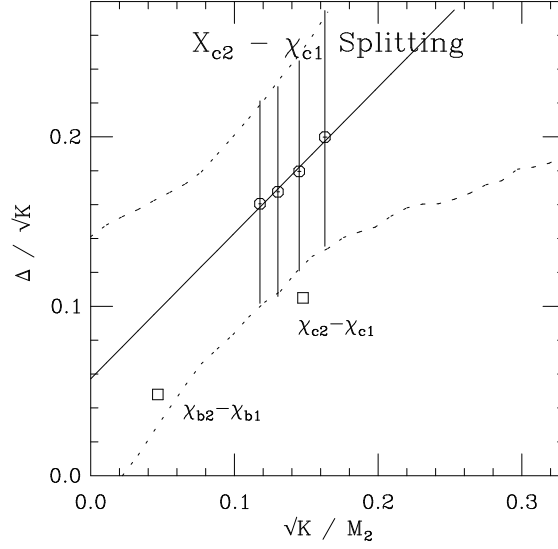


FIG. 13. Heavy quark extrapolation of quarkonium  $\chi_{c2} - \chi_{c0}$  fine splitting at  $\beta = 6.0$  in a similar manner to figure 12. The axes are scaled using the string tension.

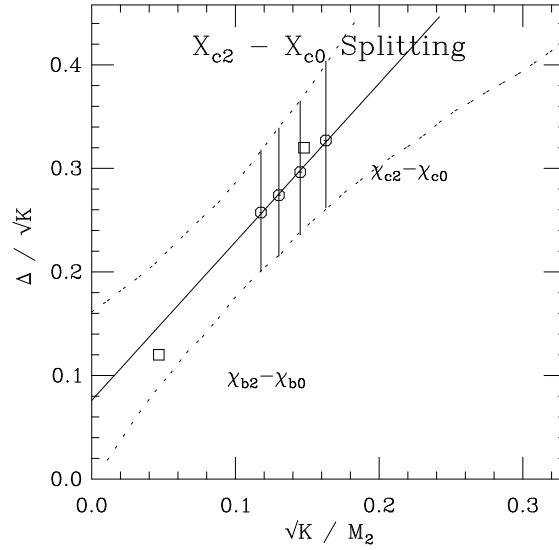


FIG. 14. Charmonium spectrum diagram using the string tension to set the scale at  $\beta = 6.0$ . Broad agreement is seen, but it appears that the spin structure is underestimated.

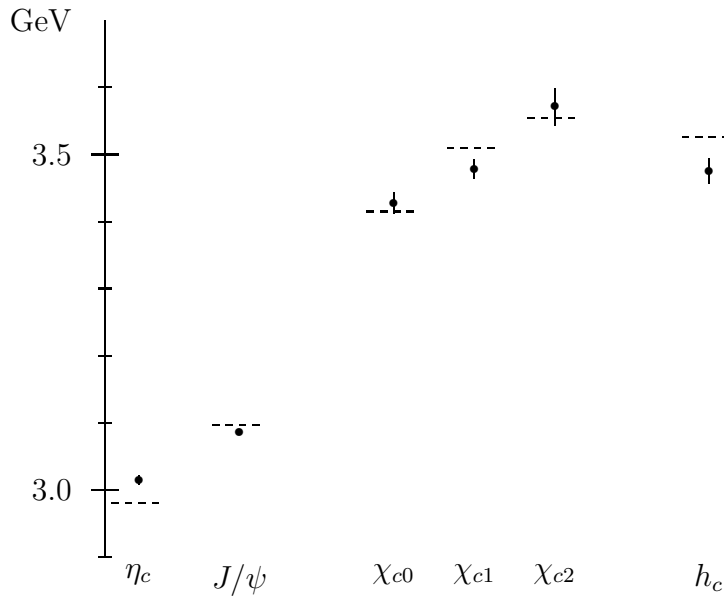


FIG. 15. Upsilon spectrum diagram using string tension to set scale at  $\beta = 6.0$ . Clearly the  $S-P$  splitting is underestimated when using the same scale as the charmonium simulation. This effect is universally believed to be due to quenching. It is commonly absorbed by using the S-P splitting to set the scale in a system dependent manner, which would involve a loss of predictive power here. Presenting our data in this manner shows that any single quenched theory cannot simultaneously get both spectra correct.

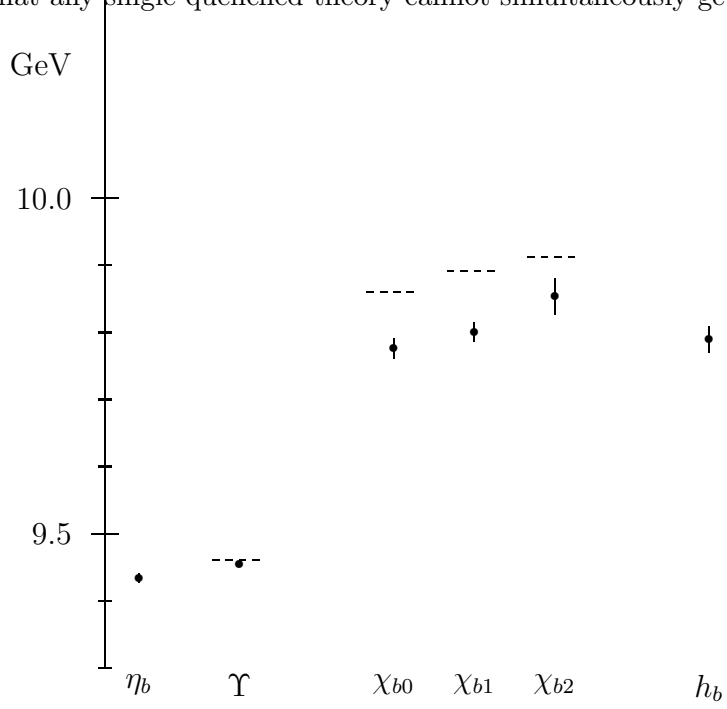


FIG. 16. Scaling behaviour of  $J/\psi$  and  $\Upsilon$  hyperfine splitting between  $\beta = 6.0$  and  $\beta = 6.2$ . Results scale well with both the string tension and  $M_\rho$ . We have no value for the  $S - P$  splitting at  $\beta = 6.2$ ; it is possible that one would obtain results with  $S - P$  which scale, but yield different continuum limit (particularly for  $\Upsilon$ ), the discrepancy being a quenching error.

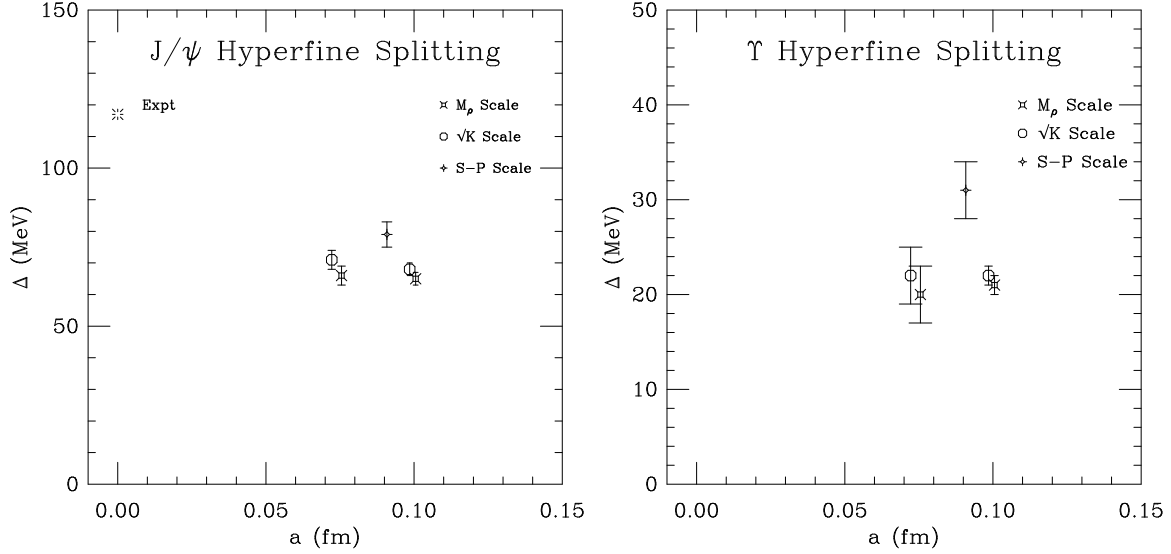
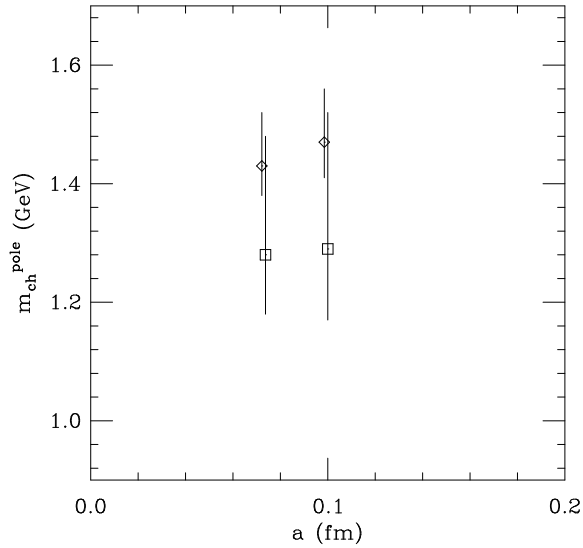


FIG. 17. Scaling Behaviour of  $m_{\text{charm}}^{\text{pole}}$ . The error here is dominated by the uncertainty in  $q^*$ . It is plausible that the results from the method 1 (diamonds) and method 2 (squares) will agree in the continuum limit.





TABLES

TABLE I.  $\beta = 6.0$  heavy quark kappas

$\kappa$	$aM_{PS}(Q\bar{Q})$	Fuzzing Radius	MR Iterations
0.13000	0.9283(7)	3	95
0.12600	1.1618(6)	3	75
0.12200	1.3755(6)	3	65
0.11800	1.5751(6)	3	60
0.11400	1.7644(6)	3	55

TABLE II. Meson operators

State	$J^{PC}$	Operators
$^1S_0$	$0^{-+}$	$\bar{\psi}\gamma_5\psi$
$^3S_1$	$1^{--}$	$\bar{\psi}\gamma_i\psi$
$^1P_1$	$1^{+-}$	$\bar{\psi}\sigma_{ij}\psi, \bar{\psi}\gamma_5\Delta_i\psi$
$^3P_0$	$0^{++}$	$\bar{\psi}\psi, \bar{\psi}\sum\gamma_i\Delta_i\psi$
$^3P_1$	$1^{++}$	$\bar{\psi}\gamma_i\gamma_5\psi, \bar{\psi}\{\gamma_i\Delta_j - \gamma_j\Delta_i\}\psi$
$^3P_2$	$2^{++}$	$\bar{\psi}\{\gamma_i\Delta_i - \gamma_j\Delta_j\}\psi$ E rep $\bar{\psi}\{\gamma_i\Delta_j + \gamma_j\Delta_i\}\psi$ T rep

TABLE III.  $\beta = 6.0$  fitted timeslice ranges

State	Pseudoscalar	Vector	P-states
Fit Range	8-20 (FL,LL)	8-20 (FL,LL)	6-18 (FL,LL)

TABLE IV. Heavy-heavy S states

State	$\chi^2/dof$	Q	$M_{GS}$	$M_{EX}$
Pseudo (3000,3000)	0.83	0.68	0.9283(7)	1.41(3)
Pseudo (2600,2600)	0.88	0.61	1.1619(6)	1.60(2)
Pseudo (2200,2200)	0.99	0.47	1.3755(6)	1.79(2)
Pseudo (1800,1800)	1.2	0.25	1.5751(6)	1.97(1)
Pseudo (1400,1400)	1.4	0.093	1.7644(6)	2.14(1)
Vector (3000,3000)	1.0	0.44	0.9780(9)	1.49(2)
Vector (2600,2600)	0.95	0.52	1.1990(8)	1.66(2)
Vector (2200,2200)	1.0	0.44	1.4052(7)	1.83(1)
Vector (1800,1800)	1.2	0.26	1.5998(7)	2.00(1)
Vector (1400,1400)	1.4	0.12	1.7854(7)	2.17(1)

TABLE V. Heavy-heavy P states

State	$\chi^2/dof$	Q	$M_{GS}$	$M_{EX}$
$0^{++}$ (3000,3000)	1.1	0.37	1.161(7)	1.76(10)
$0^{++}$ (2600,2600)	0.92	0.56	1.376(7)	1.89(7)
$0^{++}$ (2200,2200)	0.91	0.57	1.578(6)	2.04(5)
$0^{++}$ (1800,1800)	1.0	0.45	1.770(6)	2.19(4)
$0^{++}$ (1400,1400)	1.2	0.28	1.955(7)	2.34(4)
$1^{++}$ (3000,3000)	0.62	0.90	1.193(7)	1.76(7)
$1^{++}$ (2600,2600)	0.56	0.94	1.404(7)	1.91(6)
$1^{++}$ (2200,2200)	0.65	0.87	1.602(6)	2.07(5)
$1^{++}$ (1800,1800)	0.79	0.73	1.791(7)	2.22(4)
$1^{++}$ (1400,1400)	0.91	0.58	1.972(7)	2.37(4)
$1^{+-}$ (3000,3000)	0.56	0.94	1.193(8)	1.67(6)
$1^{+-}$ (2600,2600)	0.42	0.99	1.402(7)	1.86(5)
$1^{+-}$ (2200,2200)	0.51	0.96	1.602(7)	2.04(5)
$1^{+-}$ (1800,1800)	0.70	0.83	1.792(7)	2.21(4)
$1^{+-}$ (1400,1400)	0.86	0.64	1.975(7)	2.37(4)

TABLE VI. Momenta or kinetic mass analyses

Momentum Directions		
	(0,0,0)	
(1,0,0)	(0,1,0)	(0,0,1)
(1,1,0)	(1,0,1)	(0,1,1)
	(1,1,1)	
(2,0,0)	(0,2,0)	(0,0,2)

 TABLE VII. Heavy-heavy  $M_2(PS)$ 

State	$\chi^2/dof$	$M_2$
Pseudo (3000,3000)	1.0	1.024(11)
Pseudo (2600,2600)	0.14	1.350(11)
Pseudo (2200,2200)	0.14	1.686(12)
Pseudo (1800,1800)	0.6	2.05(1)
Pseudo (1400,1400)	0.9	2.43(1)
Pseudo (2600,1400)	0.12	1.87(1)
Pseudo (2600,1800)	0.06	1.69(1)
Pseudo (2600,2200)	0.025	1.51(1)

 TABLE VIII.  $\beta = 6.0$  heavy-heavy mass splittings

Splitting (MeV)	$\sqrt{K}$	$M_\rho$	$Q\bar{Q}$ S-P Splitting	Experiment
$J/\psi - \eta_c$	68(2)	65(2)	79(4)	117
$^1P_1 - \bar{S}$	418(13)	408(16)	-	458
$\chi_{c2} - \chi_{c1}$	81(28)	78(27)	93(33)	46
$\chi_{c1} - \chi_{c0}$	51(7)	49(7)	59(11)	95
$\chi_{c2} - \chi_{c0}$	133(28)	128(28)	153(35)	141
$\Upsilon - \eta_b$	22(1)	21(1)	31(3)	-
$^1P_1 - \bar{S}$	366(17)	358(20)	-	460
$\chi_{b2} - \chi_{b1}$	43(30)	42(30)	56(32)	21
$\chi_{b1} - \chi_{b0}$	26(9)	25(9)	33(10)	32
$\chi_{b2} - \chi_{b0}$	65(30)	63(27)	85(32)	53

TABLE IX.  $\beta = 6.2$  heavy-heavy mass splittings

Splitting (MeV)	$\sqrt{K}$	$M_\rho$	Experiment
$J/\psi - \eta_c$	72(3)	66(3)	117
$\Upsilon - \eta_b$	22(3)	20(3)	-